symmetry

MDPI

Article

The In-Plane-Two-Folders Symmetric *a*-Plane AlN Epitaxy on *r*-Plane Sapphire Substrate

Fabi Zhang [1], Lijie Huang [1,2], Jin Zhang [1,2], Zhiwen Liang [3], Chenhui Zhang [4], Shangfeng Liu [2,5], Wei Luo [2], Junjie Kang [2,*], Jiakang Cao [2], Tai Li [2,5], Qi Wang [3] and Ye Yuan [2,*]

1 Guangxi Key Laboratory of Precision Navigation Technology and Application, Guilin University of Electronic Technology, Guilin 541004, China; zhangfabi@outlook.com (F.Z.); 18673751825@163.com (L.H.); 18811137268@163.com (J.Z.)
2 Songshan Lake Materials Laboratory, Dongguan 523808, China; sfliu@pku.edu.cn (S.L.); luowei@sslab.org.cn (W.L.); caojiakang@sslab.org.cn (J.C.); 1901110161@pku.edu.cn (T.L.)
3 Dongguan Institute of Optoelectronics, Peking University, Dongguan 523808, China; liangzw@pku-ioe.cn (Z.L.); wangq@pku-ioe.cn (Q.W.)
4 Physical Science and Engineering Division (PSE), King Abdullah University of Science and Technology (KAUST), Thuwal 23955-6900, Saudi Arabia; chenhui.zhang@kaust.edu.sa
5 State Key Laboratory of Artificial Microstructure and Mesoscopic Physics, School of Physics, Peking University, Beijing 100871, China
* Correspondence: kangjunjie@sslab.org.cn (J.K.); yuanye@sslab.org.cn (Y.Y.)

Abstract: In the present work, a single-crystalline epitaxial nonpolar *a*-plane AlN film with in-plane two-folder symmetries was successfully achieved on an *r*-plane sapphire substrate, by combining physical vapor deposition and a high-temperature annealing technique. Moreover, by varying the AlN thickness, the evolution of crystalline quality and structure were systematically investigated using X-ray diffraction, Raman spectroscopy, and atomic force microscopy. The crystalline quality was much improved by the annealing treatment. Most importantly, when the thickness of AlN was increased up to 1000 nm, the AlN lattice was found to endure strong distortion along the out-of-plane direction, and the lattice showed an obvious expansion. The change of the surface morphology induced by high-temperature annealing was also tracked, and the morphology displayed structural anisotropy along the $[1\bar{1}00]$ direction. Our results act as a crucial platform to better understand and employ the nonpolar AlN template; in particular, it is of importance for subsequent device fabrication.

Keywords: nonpolar; *a*-plane AlN; *r*-plane sapphire

Citation: Zhang, F.; Huang, L.; Zhang, J.; Liang, Z.; Zhang, C.; Liu, S.; Luo, W.; Kang, J.; Cao, J.; Li, T.; et al. The In-Plane-Two-Folders Symmetric *a*-Plane AlN Epitaxy on *r*-Plane Sapphire Substrate. *Symmetry* **2022**, *14*, 573. https://doi.org/10.3390/sym14030573

Academic Editor: Enrique Maciá Barber

Received: 21 February 2022
Accepted: 8 March 2022
Published: 14 March 2022

1. Introduction

In the past decades, the development of GaN based light-emitting diode (LED) and laser devices has thoroughly revolutionized human luminescence history [1–5]. However, several intrinsic properties, of both material and physics aspects, still act as disadvantages to block their further develop. One of the significant reasons is the strong polarization induced by the quantum confined stark effect (QCSE), which causes the deviation of carrier wave function along the c-axis [6,7]: the spontaneous polarization along the [0001] direction in a conventional LED sets up an electric field that undesirably impedes the carrier recombination in the quantum well region [6–8]. In particular, such a phenomenon gradually dominates upon increasing the c-axis polarization contribution, e.g., it is obviously enhanced when aluminum concentration is increased in an AlGaN compound [9–11]. This is detrimental to luminance devices with a high Al concentration, e.g., an LED or laser in the ultraviolet-C region (UVC band, wavelength < 280 nm) [10]. Moreover, in UVC–LED devices, such intensive polarization results in high TM luminance mode, which transfers a large part of emissions from the plane to edge region; thus, this again reduces the emission of the device [12,13]. It is worth noting that, under the above-mentioned influences, the UVC–LEDs normally exhibit a wall plug efficiency (WPE) less than 10%, which is far from

the value of a GaN based blue-LED [11,14]. Therefore, exploring a strategy to reduce the polarization field is of great interest, to further develop UVC luminance devices.

In fact, utilizing the non-polar or semi-polar face of a nitride semiconductor has been proven effective to improve the performance of luminance devices in the visible band, through avoiding the polarization field. For instance, Nakamura's group reported excellent lighting efficiency by employing a semipolar $(20\bar{2}\bar{1})$ and $(10\bar{1}\bar{1})$ InGaN/GaN LED [15,16]; a green LED on $(11\bar{2}\bar{2})$ a free-standing GaN template also presented the advantages of high power and high efficiency [17]. Therefore, it is expected that the strategy of a non-polar or semi-polar sapphire substrate will be introduced into UVC–LEDs, due to the UVC-transparent characteristics of sapphire substrates, and plenty of studies have been carried out into the preparation of various types of non-polar AlN templates on sapphire substrates [18–24]. Recently, the technique of high temperature annealing has become attractive, due to its success in improving c-plane AlN template quality and the corresponding UVC–LEDs [25–27]; thus, it makes senses that such a strategy is employed in the preparation of a non-polar AlN template.

In the present work, by fully combining physical vapor deposition and a high temperature annealing technique, we successfully achieve a single-crystalline non-polarized *a*-plane AlN on a semi-polarized *r*-plane sapphire substrate. According to systematic investigations on crystalline structure, a two-folder structural symmetry was created in the as-sputtered *a*-plane AlN on an *r*-plane sapphire substrate. Moreover, the high temperature annealing operation greatly improved the crystalline quality and reset the strain statues in the as-sputtered samples. In particular, upon increasing AlN thickness, a crystalline distortion along the out-of-plane direction was found to present a strain evolution. As a result, our results act as a solid and meaningful example for lateral research on non-polar nitride semiconductors based LEDs, by fully employing the structural symmetry of a nitride semiconductor.

2. Experiment

2.1. Synthesis

The AlN templates were prepared on *r*-plane sapphires by physical vapor deposition (PVD). The aluminum (purity ~ 99.999%) was the target, and the sputtering ambience was a mixture of argon and nitrogen, at a ratio of 1:4. The sputtered AlN was 500 nm, by calibrating the growth speed, and the sputtering power and temperature were 3000 W and 500 °C, respectively. Afterwards, the as-grown AlN templates were annealed in a tube furnace at 1700 °C for 5 h, and the annealing ambience was nitrogen.

2.2. X-ray Diffraction (XRD) Characterization

The X-ray diffraction rocking curves of AlN (100) and (110) planes, 2theta-omega, and phi scans were measured using X-ray diffraction (XRD, Brucker D8 Discovery), to obtain the AlN crystalline information. A Cu target was used to excite the $K_{\alpha 1}$ X-ray, with λ = 0.154056 nm.

2.3. Atomic Force Microscopy (AFM) Characterization

Atomic force microscopy (AFM, Veeco Dimension TM 3100) with a typing mode was used to explore the surface morphology of all AlN samples.

2.4. Raman Spectroscopy Characterization

Raman spectroscopy was performed using a LabRam HR Evolution microscopic confocal Raman spectrometer from Horiba. The micro-Raman spectroscopy was excited by 532 nm laser, and the laser beam was focused on a spot size about 0.7 μm in diameter.

3. Result and Discussion

Figure 1 shows the crystalline quality of the as-grown and annealed AlN samples using an X-ray diffraction rocking curve, in order to evaluate the contribution of high

temperature annealing to lattice reordering. Therefore, (110) and (100) crystalline planes were selected to explore the crystalline order along the out-of-plane and in-plane components, respectively. Before the high temperature annealing operation, both planes did not present any diffraction peaks, indicating poor crystallinity. However, the annealing treatment triggered the crystallization of the lattice, and, accordingly, both planes displayed strong diffraction peaks in the X-ray diffraction rocking curves. The full width at half maximums (FWHM) of the (110) and (100) plane rocking curves were 0.36° and 0.42°, respectively. According to a previous study, the quality of our *a*-AlN is comparable with an MOVPE grown *a*-AlN at the optimal temperature of 1250 °C [28]. However, it is worth noting that it seems that the annealing time does have an influence on the crystallinity of nonpolar AlN templates. According to the study from Chia-Hung Lin et al. [21], an annealing time of only 10 min at 1700 °C produced an outstanding crystalline quality, with (110) and (002) FWHMs of 770 and 640 arcsec, respectively. Actually, the crystallinity is strongly dependent on the layer thickness, due to the effect of the AlN–sapphire interface. In Figure 1c, the thickness dependent FWHMs of both planes are plotted for analysis. The 500-nm thick sample exhibits the best crystal quality, probably as the main AlN part is away from the interface.

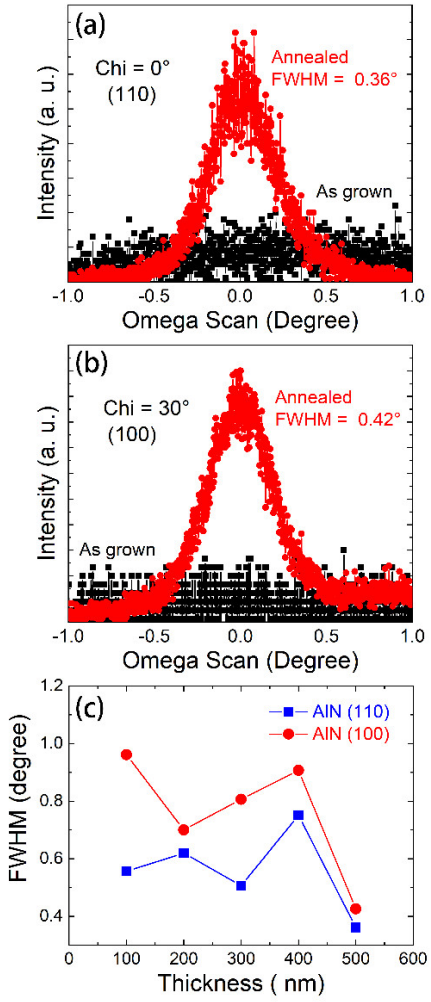

Figure 1. XRD rocking curves of (**a**) (110) and (**b**) (100) planes of as-grown and annealed 500 nm thick samples; (**c**) thickness-dependent FWHMs of (110) and (100) plane rocking curves of annealed AlN samples.

For the out-of-plane direction, the coexistence of the sapphire (012), (024), (036), and AlN (110) plane diffractions can be clearly observed, which indicates the epitaxial relation

of the *a*-plane AlN on *r*-face sapphire. For the as-grown sample, the AlN (110) peak is broad and noisy, whereas the annealing treatment intensively sharpens the diffraction peak, indicating an improvement in crystallinity. Moreover, after the high-temperature operation, the diffraction of the (100) plane with in-plane component started to appear when the measured Chi was set as 30°, as shown in Figure 2b. As presented in Figure 2c, calibrated by the sapphire (024) diffraction peak, the annealed *a*-plane AlN films present almost the same diffraction position at 2θ = 59.19° as the (110) plane, when the thickness is below 500 nm. However, the (110) plane diffraction shifted towards the small angle side at 2θ = 59.05° for the 1000 nm thick sample, suggesting that lattice expansion occurred. The lattice parameter was calculated as 1.5640 Å for the 1000-nm thick sample, which is larger than the value of 1.5608 Å in the other samples. According to a previous study [29], an MOCVD grown 1000-nm thick AlN exhibited a (110) diffraction peak at 2θ = 59.4°, which means that the annealed AlN sample exhibited larger lattice parameters than an MOCVD grown sample. Such a difference is probably due to the ultra-high temperature treatment inducing an intensive compressive strain in the annealed sample.

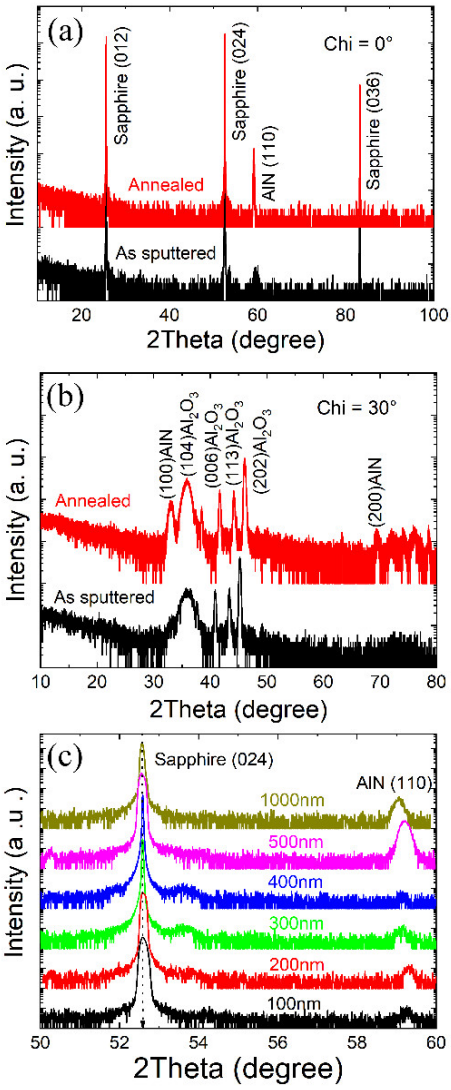

Figure 2. XRD 2Theta-Omega scans of as-grown and annealed samples, when the scanning directions are along the AlN (**a**) out-of-plane $[11\bar{2}0]$ and (**b**) specific $[1\bar{1}00]$ directions; (**c**) the 2Theta-Omega scans along the $[11\bar{2}0]$ direction of annealed AlN samples with different thicknesses.

Figure 3 shows the Raman spectra of annealed samples with different thicknesses, and various phonon vibration modes were investigated. The measurements were carried

out under natural light excitation; therefore, consideration of polarized vibration was not needed. As shown in Figure 3a, for annealed samples with different thicknesses, the coexistence of sapphire and AlN signals was observed. In all samples, various sapphire vibration phonons were observed at positions of 378.5, 415.5, 429.6, 575.7, and 749.8 cm^{-1}. For AlN film, three vibration peaks were seen: the A_1(TO), E_2^H, and E_1(TO) modes at around 644.2, 663.2, and 675.8 cm^{-1}; the corresponding vibration mode schemes are shown in Figure 3b. The appearance of all Raman signals indicates the good crystallinity of the annealed samples.

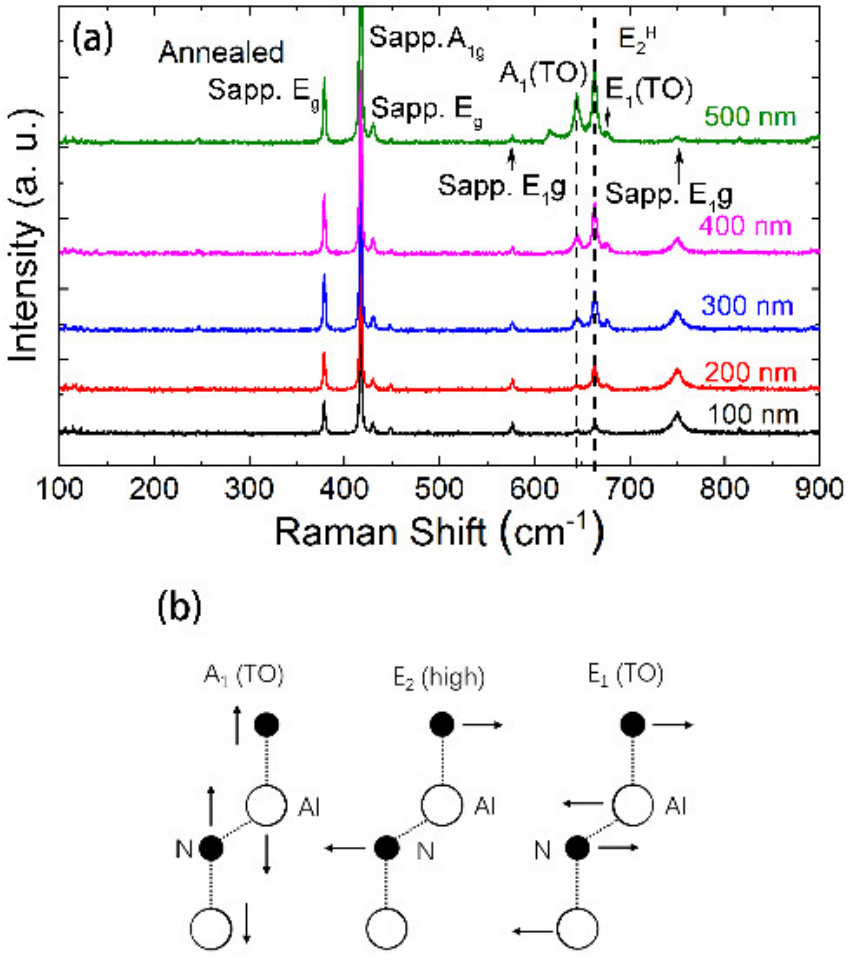

Figure 3. (**a**) The full Raman spectra of annealed samples with different thicknesses, and the phonon vibration signals of the sapphire substrate and AlN epilayer are labelled; (**b**) the scheme of different phonon vibration modes in the AlN lattice.

In order to show more detailed information, the AlN peak region of both the as-grown and annealed samples are both zoomed in, for a convenient reading and comparison. The Raman peaks of the annealed samples are much sharper than ones in the as-grown samples, indicating the crystalline quality was greatly improved by the annealing process. All Raman scattering peaks from the AlN fit, in terms of the Lorentzian function, and the FWHMs and Raman shifts are shown in Figure 4c,d. It is worth noting that the A_1(TO) mode did not change very much, despite it being under the annealing operation, including both the FWHM and Raman shift. In addition, it can be observed that the A_1(TO) vibration presents a redshift feature upon increasing thickness. A similar characteristic was observed in *a*-AlN with buffers grown at different temperatures, which resulted from the introduced strain [30,31]. However, the HTA had an obvious contribution to the E_2^H peak, and it can be noted that both the FWHM and Raman wavenumber were greatly decreased by HTA. The FWHM reduction mainly resulted from the improvement of crystalline quality; however,

the decreased Raman wavenumber was caused by the strain resetting after annealing. When compared with the strain-free $E_2{}^H$ signal at 657 cm^{-1} in bulk AlN, our as-grown *a*-AlNs present a blueshift, while the annealed samples exhibit a redshift. According to previous studies [32], the phonon frequency reduction and increase are caused by the lattice expansion and shrinkage, respectively. The Raman results are in agreement with the XRD 2Theta-Omega scans.

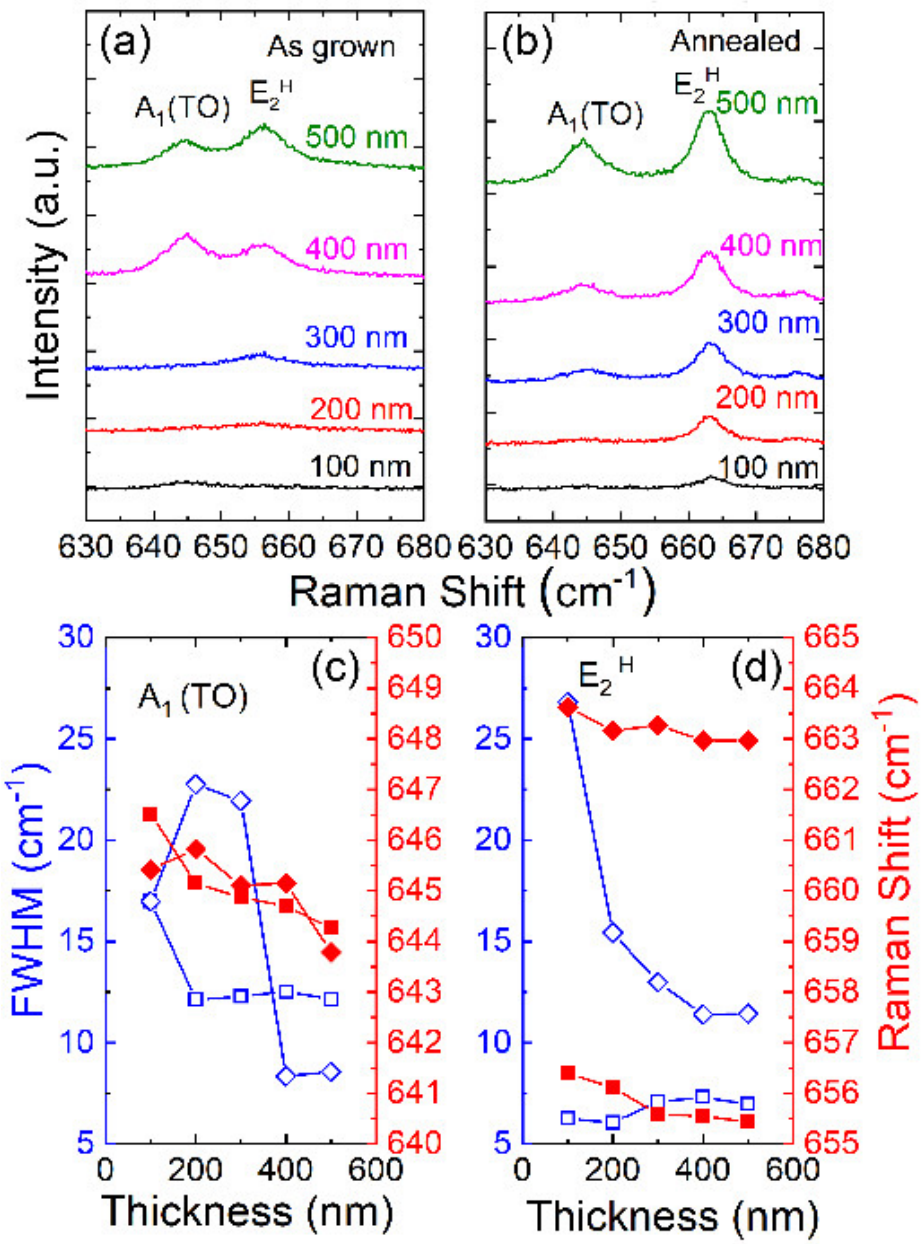

Figure 4. The region of Raman spectra from 630 to 680 cm^{-1} of (**a**) as-grown and (**b**) annealed samples; the FWHM (blue open labels) and Raman shift (red solid labels) of (**c**) A_1(TO) and (**d**) $E_2{}^H$ modes, as dependent on the thickness of the as-grown (diamonds) and annealed (squares) samples.

The epitaxial relation between *r*-plane sapphire and *a*-plane AlN film is presented in Figure 5. According to the phi scans in Figure 5a, when the Chi was set as 57.61° and 30.66°, respectively, peaks from the sapphire (006) and AlN (100) planes were visible. The phi positions of the two diffraction peaks are both vertical, indicative that the in-plane component of the *r*-sapphire c-axis is parallel with the c axis of *a*-AlN. Such a phenomenon is consistent with previous studies on AlN and *r*-sapphire substrates [33–35].

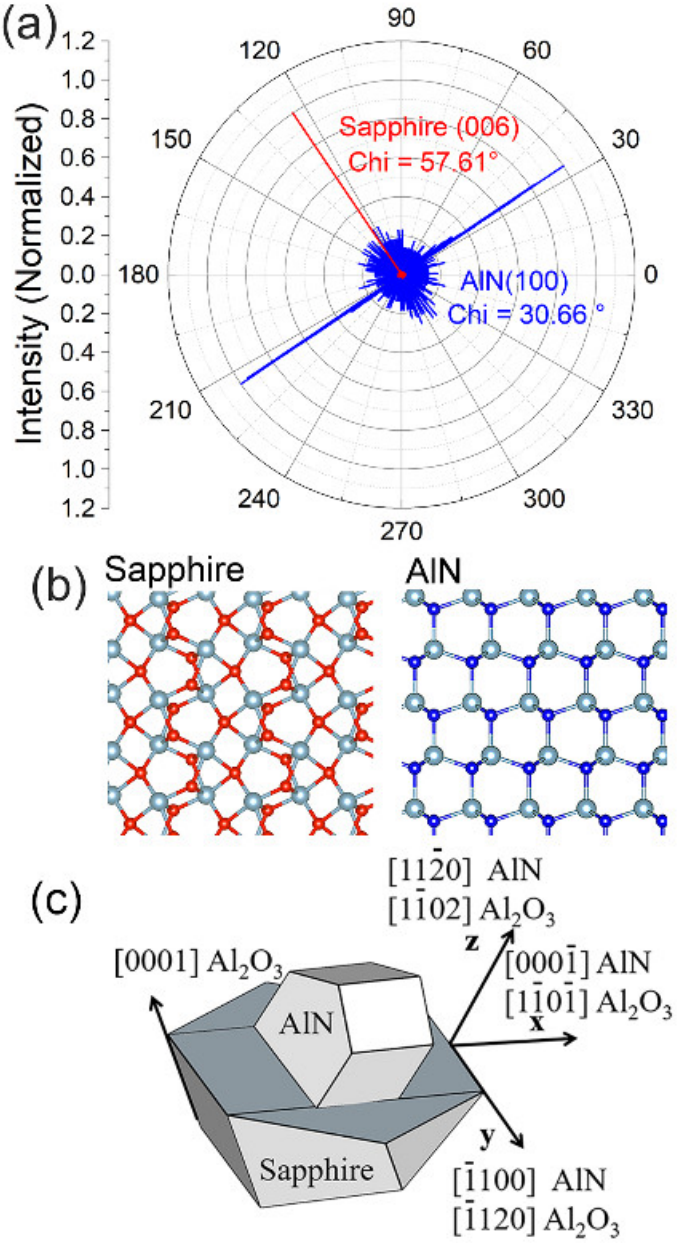

Figure 5. (**a**) The XRD phi-dependent polar figures of *r*-sapphire substrate (006) and *a*-AlN (100) film, it is clearly observed that the in-plane components of the AlN and sapphire are both vertical. (**b**) The lattice scheme of the *a*-AlN and *r*-sapphire from the out-of-plane direction (*r*-direction of sapphire and *a*-direction of AlN); (**c**) three-dimensional crystalline scheme of the epitaxial relationship between the sapphire substrate and AlN epilayer.

The detailed epitaxial structure between the *a*-AlN and *r*-sapphire substrate is shown in Figure 6. Unexpectedly, when a Chi scan was carried out to examine the (100) plane, the value of the Chi angle continuously reduced upon increasing the thickness. In particular, after being calibrated by the sapphire miscut angle and AlN out-of-plane $[11\bar{2}0]$ direction, the Chi angle was as small as 25.4° when the thickness was 1000 nm. This is smaller than 28.0° in the 500-nm thick sample and the ideal 30° in the strain-free case, as shown in Figure 6a. Such a difference indicates a uniaxial structural distortion in the lattice, and this is presented in Figure 6b.

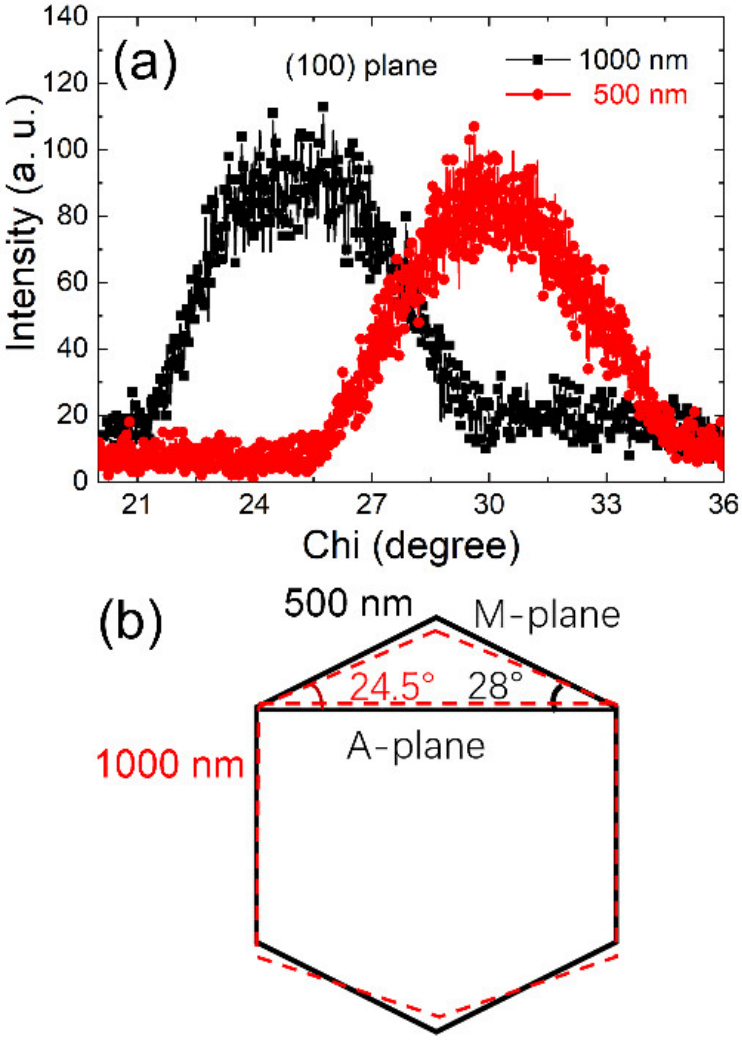

Figure 6. (**a**) Chi scans of the (100) plane of AlN samples with 500 and 1000 nm thickness after calibrating the $[11\bar{2}0]$ direction of the sapphire substrates; (**b**) the corresponding scheme of lattice distortion describe in (**a**).

In order to investigate the surface morphology, we employed atomic force microscopy for the as-grown and annealed *a*-AlN, for a comparison. Unlike the conventional c-AlN on c-sapphire, which presents a particle-like morphology, the as-grown *a*-AlN shows an obvious lattice-direction oriented morphology along the AlN $[1\bar{1}00]$ direction. The growth mode of the as sputtered AlN layer has a typical three-dimensional (3D) growth before thermal annealing, due to the lack of sufficient Al immigration during the low temperature sputtering process. The root mean square (RMS) index was calculated as 4.9 nm. Subsequently, the annealing operation activated the merging of the micro-crystals, and it can ce observed in Figure 7b that the crystal size became larger and the $[1\bar{1}00]$ oriented feature is much more obvious. However, a similar morphology was observed in *a*-GaN or *a*-AlN on *r*-sapphire substrate by MOCVD; however, the surface from the MOCVD grown sample was flatter than the sample herein [18,36]. Actually, the selection of preparation conditions can modulate the morphology, e.g., the employment of a three-step pulsed flow growth method can suppress the appearance of such a surface by MOCVD [31]. Interestingly, for the hydride vapor phase epitaxy (HVPE) grown sample, the as-grown sample presented an obvious anisotropy morphology when it was prepared at 900 °C, and this strip-like form was retained during the 1600~1700 °C annealing [21]. However, in our case, the annealed sample presented 9.6 nm RMS, which is twice the value of the as-grown sample, which was probably due to the surface decomposition during the annealing

operation, although the Al immigration was ensured in such a high temperature treatment. Therefore, it is particularly worth noting that in order to avoid a negative contribution from the morphology, the surface decomposition has to be considered.

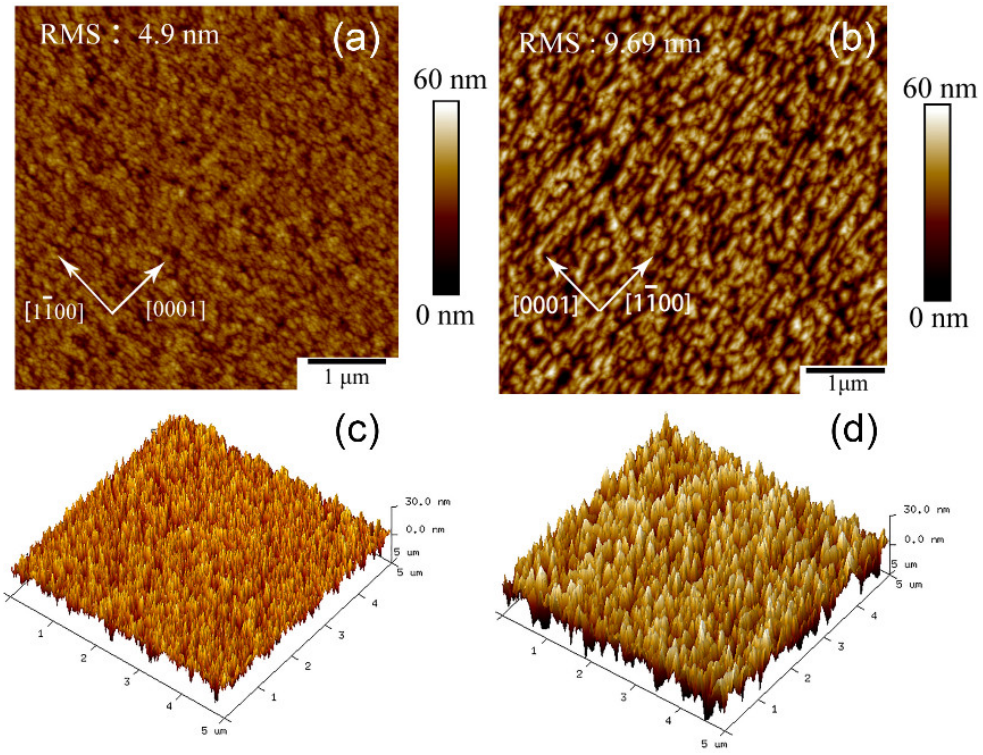

Figure 7. The AFM images of (**a**,**c**) as-grown and (**b**,**d**) annealed samples.

The evolution of the AlN lattice and morphology is critically important for subsequent device epitaxy. The crystalline state determines the dislocation behavior and strain in the upper device, including dislocation generation, movement, merging, and annihilation. The strain state not only works through the above-mentioned dislocation features, it also contributes to the device performance via energy band modulation. The morphology has a great effect on nucleation in the subsequent epitaxy process; therefore, acting as an important base, which has to be considered for the upper device design and growth. When compared with the other studies of *a*-AlN, our investigation mainly focused on the crystalline information; moreover, we also initially explored the large lattice distortion along the out-of-plane direction upon increasing the AlN thickness.

4. Conclusions

In summary, through combing physics vapor deposition and a high-temperature annealing technique, we successfully prepared an in-plane two-folder symmetric epitaxial nonpolar *a*-plane AlN on a semipolar *r*-plane sapphire substrate. The high-temperature annealing intensively reordered the lattice; therefore, improving the crystalline quality of the as-sputtered AlN film. According to systematic studies by XRD, Raman, and AFM, the post-annealed lattice can endure expansion upon gradually increasing the AlN thickness. In particular, it was found that a large thickness of around 1000 nm leads to adverse stretching along the out-of-plane direction, according to the XRD results. When compared with other conventional template materials, e.g., c-AlN, which exhibits intensive polarization along the out-of-plane direction, the specific in-plane two-fold symmetric structure confirms the successful preparation of a non-polar AlN template, and has potential to enhance the emission performance along the out-of-plane direction in optoelectronic devices.

Author Contributions: Data curation, L.H., J.Z. and C.Z.; Formal analysis, S.L.; Investigation, W.L. and J.C.; Project administration, J.K.; Resources, T.L.; Software, Z.L.; Supervision, Y.Y.; Writing—original draft, F.Z.; Writing—review & editing, Q.W. All authors have read and agreed to the published version of the manuscript.

Funding: This work was partly supported by the National Key R&D Program of China (No. 2021YFA0716400). This work was supported by the Guangdong Basic and Application Basic Research Foundation of Guangdong Province (Nos. 2021B1515120022, 2020A1515110891, 2019B1515120091 and 2019B1515120081). The author Fabi Zhang was sponsored by the Guangxi Scholarship Fund of Guangxi Education Department.

Data Availability Statement: Not applicable.

Conflicts of Interest: The authors declare no conflict of interest.

References

1. Nanishi, Y. The birth of the blue LED. *Nat. Photonics* **2014**, *8*, 884–886. [CrossRef]
2. Amano, H.; Kito, M.; Hiramatsu, K.; Akasaki, I. P-Type Conduction in Mg-Doped GaN Treated with Low-Energy Electron Beam Irradiation (LEEBI). *Jpn. J. Appl. Phys.* **1989**, *28*, L2112. [CrossRef]
3. Nakamura, S.; Senoh, M.; Nagahama, S.-I.; Iwasa, N.; Yamada, T.; Matsushita, T.; Kiyoku, H.; Sugimoto, Y. InGaN-Based Multi-Quantum-Well-Structure Laser Diodes. *Jpn. J. Appl. Phys.* **1996**, *35*, L74. [CrossRef]
4. Nakamura, S.; Mukai, T.; Senoh, M. High-Power GaN P-N Junction Blue-Light-Emitting Diodes. *Jpn. J. Appl. Phys.* **1991**, *30*, L1998. [CrossRef]
5. Nakamura, S.; Senoh, M.; Iwasa, N.; Nagahama, S.-i. High-Brightness InGaN Blue, Green and Yellow Light-Emitting Diodes with Quantum Well Structures. *Jpn. J. Appl. Phys.* **1995**, *34*, L797. [CrossRef]
6. Takeuchi, T.; Sota, S.; Katsuragawa, M.; Komori, M.; Takeuchi, H.; Amano, H.; Akasaki, I. Quantum-Confined Stark Effect due to Piezoelectric Fields in GaInN Strained Quantum Wells. *Jpn. J. Appl. Phys.* **1997**, *36*, L382. [CrossRef]
7. Leroux, M.; Grandjean, N.; Laügt, M.; Massies, J.; Gil, B.; Lefebvre, P.; Bigenwald, P. Quantum confined Stark effect due to built-in internal polarization fields in (Al,Ga)N/GaN quantum wells. *Phys. Rev. B* **1998**, *58*, R13371(R). [CrossRef]
8. Masui, H.; Sonoda, J.; Pfaff, N.; Koslow, I.; Nakamura, S.; DenBaars, S.P. Quantum-confined Stark effect on photoluminescence and electroluminescence characteristics of InGaN-based light-emitting diodes. *J. Phys. D Appl. Phys.* **2008**, *41*, 165105. [CrossRef]
9. Guo, Q.; Kirste, R.; Mita, S.; Tweedie, J.; Reddy, P.; Washiyama, S.; Breckenridge, M.H.; Collazo, R.; Sitar, Z. The polarization field in Al-rich AlGaN multiple quantum wells. *Jpn. J. Appl. Phys.* **2019**, *58*, SCCC10. [CrossRef]
10. Schlichting, S.; Hönig, G.M.O.; Müßener, J.; Hille, P.; Grieb, T.; Westerkamp, S.; Teubert, J.; Schörmann, J.; Wagner, M.R.; Rosenauer, A.; et al. Suppression of the quantum-confined Stark effect in polar nitride heterostructures. *Commun. Phys.* **2018**, *1*, 48. [CrossRef]
11. Kneissl, M.; Seong, T.-Y.; Han, J.; Amano, H. The emergence and prospects of deep-ultraviolet light-emitting diode technologies. *Nat. Photonics* **2019**, *13*, 233–244. [CrossRef]
12. Reich, C.; Guttmann, M.; Feneberg, M.; Wernicke, T.; Mehnke, F.; Kuhn, C.; Rass, J.; Lapeyrade, M.; Einfeldt, S.; Knauer, A.; et al. Strongly transverse-electric-polarized emission from deep ultraviolet AlGaN quantum well light emitting diodes. *Appl. Phys. Lett.* **2015**, *107*, 142101. [CrossRef]
13. Li, Y.; Wang, C.; Zhang, Y.; Hu, P.; Zhang, S.; Du, M.; Su, X.; Li, Q.; Yun, F. Analysis of TM/TE mode enhancement and droop reduction by a nanoporous n-AlGaN underlayer in a 290 nm UV-LED. *Photonics Res.* **2020**, *8*, 806–811. [CrossRef]
14. Kashima, Y.; Maeda, N.; Matsuura, E.; Jo, M.; Iwai, T.; Morita, T.; Kokubo, M.; Tashiro, T.; Kamimura, R.; Osada, Y. High external quantum efficiency (10%) AlGaN-based deep-ultraviolet light-emitting diodes achieved by using highly reflective photonic crystal on p-AlGaN contact layer. *Appl. Phys. Express* **2018**, *11*, 012101. [CrossRef]
15. Feezell, D.F.; Speck, J.S.; DenBaars, S.P.; Nakamura, S. Semipolar $(20\bar{2}1)$ InGaN/GaN Light-Emitting Diodes for High-Efficiency Solid-State Lighting. *J. Disp. Technol.* **2013**, *9*, 190–198. [CrossRef]
16. Zhao, Y.; Sonoda, J.; Pan, C.-C.; Brinkley, S.; Koslow, I.; Fujito, K.; Ohta, H.; DenBaars, S.P.; Nakamura, S. 30-mW-Class High-Power and High-Efficiency Blue Semipolar (1011) InGaN/GaN Light-Emitting Diodes Obtained by Backside Roughening Technique. *Appl. Phys. Express* **2010**, *3*, 102101. [CrossRef]
17. Sato, H.; Tyagi, A.; Zhong, H.; Fellows, N.; Chung, R.B.; Saito, M.; Fujito, K.; Speck, J.S.; DenBaars, S.P.; Nakamura, S. High power and high efficiency green light emitting diode on free-standing semipolar $(11\bar{2}2)$ bulk GaN substrate. *Phys. Stat. Sol. (RRL)* **2007**, *1*, 162–164. [CrossRef]
18. Jinno, D.; Otsuki, S.; Niimi, T.; Sugimori, S.; Daicho, H.; Iwaya, M.; Takeuchi, T.; Kamiyama, S.; Akasaki, I. Annealing of the sputtered AlN buffer layer on r-plane sapphire and its effect on a-plane GaN crystalline quality. *Phys. Stat. Sol (b)* **2017**, *254*, 1600723. [CrossRef]
19. Dinh, D.V.; Hu, N.; Honda, Y.; Amano, H.; Pristovsek, M. High-temperature thermal annealing of nonpolar (100) AlN layers sputtered on (100) sapphire. *J. Cryst Growth* **2018**, *498*, 377–380. [CrossRef]
20. Jo, M.; Hirayam, H. Growth of non-polar a-plane AlN on r-plane sapphire. *Jpn. J. Appl. Phys.* **2016**, *55*, 05FA02. [CrossRef]

21. Lin, C.-H.; Yamashita, Y.; Miyake, H.; Hiramatsu, K. Fabrication of high-crystallinity a-plane AlN films grown on r-plane sapphire substrates by modulating buffer-layer growth temperature and thermal annealing conditions. *J. Cryst Growth* **2017**, *468*, 845–850.
22. Hayashi, Y.; Uesugi, K.; Shojiki, K.; Tohei, T.; Sakai, A.; Miyake, H. Thermal strain analysis considering in-plane anisotropy for sputtered AlN on c- and a-plane sapphire under high-temperature annealing. *AIP Adv.* **2021**, *11*, 095012. [CrossRef]
23. Yin, J.; Zhou, B.; Li, L.; Liu, Y.; Guo, W.; Talwar, D.N.; He, K.; Ferguson, I.T.; Wan, L.; Feng, Z.C. Optical and structural properties of AlN thin films deposited on different faces of sapphire substrates. *Semicond. Sci. Technol.* **2021**, *36*, 045012. [CrossRef]
24. Peng, X.; Sun, J.; Liu, H.; Li, L.; Wang, Q.; Wu, L.; Guo, W.; Meng, F.; Chen, L.; Huang, F.; et al. Structural and optical properties of AlN sputtering deposited on sapphire substrates with various orientations. *J. Semicond.* **2022**, *43*, 022801. [CrossRef]
25. Miyake, H.; Lin, C.-H.; Tokoro, K.; Hiramatsu, K. Preparation of high-quality AlN on sapphire by high-temperature face-to-face annealing. *J. Cryst Growth* **2016**, *456*, 155–159. [CrossRef]
26. Susilo, N.; Hagedorn, S.; Jaeger, D.; Miyake, H.; Zeimer, U.; Reich, C.; Neuschulz, B.; Sulmoni, L.; Guttmann, M.; Mehnke, F.; et al. AlGaN-based deep UV LEDs grown on sputtered and high temperature annealed AlN/sapphire. *Appl. Phys. Lett.* **2018**, *112*, 041110. [CrossRef]
27. Wang, D.; Uesugi, K.; Xiao, S.; Norimatsu, K.; Miyake, H. Low dislocation density AlN on sapphire prepared by double sputtering and annealing. *Appl. Phys. Express* **2020**, *13*, 095501. [CrossRef]
28. Miyagawa, R.; Miyake, H.; Hiramatsu, K. a-plane AlN and AlGaN growth on r-plane sapphire by MOVPE. *Phys. Stat. Sol (c)* **2010**, *7*, 2107–2110. [CrossRef]
29. Tahtamouni, T.A.; Sedhain, A.; Lin, J.Y.; Jiang, H.X. Growth and optical properties of a-plane AlN and Al rich AlN/AlxGa1–xN quantum wells grown on r-plane sapphire substrates. *Phys. Stat. Sol. (c)* **2008**, *5*, 1568–1570. [CrossRef]
30. Dai, Y.; Wang, W.; Gui, C.; Wen, X.; Peng, Q.; Liu, S. A first-principles study of the mechanical properties of AlN with Raman verification. *Comput. Mater. Sci.* **2016**, *112*, 342–346. [CrossRef]
31. Chen, S.; Zhang, X.; Wang, S.; Fan, A.; He, J.; Li, C.; Lu, L.; Rao, L.; Zhuang, Z.; Hu, G.; et al. High quality non-polar a-plane AlN template grown on semi-polar r-plane sapphire substrate by three-step pulsed flow growth method. *J. Alloys Compd.* **2021**, *872*, 159706. [CrossRef]
32. Kuballa, M.; Hayes, J.M.; Shi, Y.; Edgar, J.H.; Prins, A.D.; van Uden, N.W.A.; Dunstan, D.J. Raman scattering studies on single-crystalline bulk AlN: Temperature and pressure dependence of the AlN phonon modes. *J. Cryst Growth* **2001**, *231*, 391–396. [CrossRef]
33. Shibata, T.; Asai, K.; Nakamura, Y.; Tanaka, M.; Kaigawa, K.; Shibata, J.; Sakai, H. AlN epitaxial growth on off-angle R-plane sapphire substrates by MOCVD. *J. Cryst Growth* **2001**, *229*, 63–68. [CrossRef]
34. Wu, J.-J.; Okuura, K.; Fujita, K.; Okumura, K.; Miyake, H.; Hiramatsu, K. Influence of off-cut angle of r-plane sapphire on the crystal quality of nonpolar a-plane AlN by LP-HVPE. *J. Cryst Growth* **2009**, *311*, 4473–4477. [CrossRef]
35. Adachi, M.; Fukuyama, H. Non-Polar a-Plane AlN Growth on Nitrided r-Plane Sapphire by Ga–Al Liquid-Phase Epitaxy. *Phys. Stat. Sol (a)* **2018**, *255*, 1700478. [CrossRef]
36. Okada, N.; Katoa, N.; Satoa, S.; Sumiia, T.; Fujimotoa, N.; Imuraa, M.; Balakrishnana, K.; Iwayaa, M.; Kamiyamaa, S.; Amanoa, H.; et al. Epitaxial lateral overgrowth of a-AlN layer on patterned a-AlN template by HT-MOVPE. *J. Cryst Growth* **2007**, *300*, 141–144. [CrossRef]